ISPRS Journal of Photogrammetry and Remote Sensing 66 (2011) 608–619

Contents lists available at ScienceDirect

ISPRS Journal of Photogrammetry and Remote Sensing

journal homepage: www.elsevier.com/locate/isprsjprs

Land use and land cover classification over a large area in Iran based on single date analysis of satellite imagery

Hossein Saadat [a,*], Jan Adamowski [a], Robert Bonnell [a], Forood Sharifi [b], Mohammad Namdar [c], Sasan Ale-Ebrahim [c]

[a] McGill University, Macdonald Campus 21, 111 Lakeshore Road, Ste-Anne-de-Bellevue, Que., Canada H9X 3V9
[b] Soil Conservation and Watershed Management Research Institute (SCWMRI), P.O. Box 13445, Tehran, Iran
[c] Forest, Range and Watershed Management Organization, Lashgark Road, Tehran, Iran

ARTICLE INFO

Article history:
Received 15 June 2010
Received in revised form 8 April 2011
Accepted 12 April 2011
Available online 10 May 2011

Keywords:
Land use and land cover (LULC) classification
Unsupervised classification
Supervised classification
Normalized Difference Vegetation Index (NDVI)
Golestan Dam watershed

ABSTRACT

Accelerated soil erosion, high sediment yields, floods and debris flow are serious problems in many areas of Iran, and in particular in the Golestan dam watershed, which is the area that was investigated in this study. Accurate land use and land cover (LULC) maps can be effective tools to help soil erosion control efforts. The principal objective of this research was to propose a new protocol for LULC classification for large areas based on readily available ancillary information and analysis of three single date Landsat ETM+ images, and to demonstrate that successful mapping depends on more than just analysis of reflectance values. In this research, it was found that incorporating climatic and topographic conditions helped delineate what was otherwise overlapping information. This study determined that a late summer Landsat ETM+ image yields the best results with an overall accuracy of 95%, while a spring image yields the poorest accuracy (82%). A summer image yields an intermediate accuracy of 92%. In future studies where funding is limited to obtaining one image, late summer images would be most suitable for LULC mapping. The analysis as presented in this paper could also be done with satellite images taken at different times of the season. It may be, particularly for other climatic zones, that there is a better time of season for image acquisition that would present more information.

1. Introduction

Since land use and land cover (LULC) attributes in a watershed directly influence water driven erosion, knowledge of these parameters plays an important role in ranking erosion potential and in prioritizing and developing sustainable watershed and agricultural management practices (Renard et al., 1997). In many areas of Iran and in particular in the Golestan dam watershed, which is the area that was studied in this research, significant overgrazing and inappropriate land uses (LU) such as farming on steep hillsides and up-down tillage are the main contributors to soil erosion, land degradation and flooding (Japan International Cooperation Agency, 2005; Lar Consulting Engineering, 2007). These problems have significant economic ramifications through their negative impacts on available land resources, land productivity, infrastructure and water quality (Sharifi et al., 2002). Accurate LULC maps can be effective tools in aiding soil erosion control efforts. Such maps can play an important role in watershed management as a whole and help in deciding what sort of lands are capable of sustaining agriculture and which are not (Cihlar, 2000; Renschler and Harbor, 2002). Large amounts of data are required for developing such LULC maps and remote sensing can be a source of accurate, detailed information over large areas. Remotely sensed data and the potential to distinguish between different characteristics of land features from this data provides great potential for rapidly creating accurate LULC maps (Homer et al., 2004).

LULC classification is one of the most widely used applications in remote sensing. There are many approaches that have been used to correlate image data with vegetation characteristics. Over the last few decades, numerous studies have shown the efficacy of satellite imagery in characterizing vegetation types (Joshi et al., 2006; de Asis and Omasa, 2007; Focardi et al., 2008), forests (Labrecque et al., 2006; Sivanpillai et al., 2007), and crops (Cohen and Shoshany, 2002; Wardlow et al., 2007). Chust et al. (2004) evaluated the ability of morphological indices and landscape analysis to test the improvement of land cover (LC) classification reliability in a mountainous area. They were able to define 12 LC categories using an image segmentation method (based on edge detection originated by abrupt changes in the intensity of neighboring pixels) and a supervised classification (maximum likelihood classi-

* Corresponding author. Fax: +1 5143988387.
E-mail address: hsaadat83@yahoo.ca (H. Saadat).

0924-2716/$ - see front matter © 2011 International Society for Photogrammetry and Remote Sensing, Inc. (ISPRS). Published by Elsevier B.V. All rights reserved.
doi:10.1016/j.isprsjprs.2011.04.001

fication) of a Landsat Thematic Mapper (TM) satellite image. In addition, Hagner and Reese (2007) calibrated the maximum likelihood method for classification of nine primary forest types in the CORINE land cover mapping project.

Several vegetation indices that combine reflectance of two or more wavelengths in different ways have been developed and used in characterizing vegetation growth and development (Jackson and Huete, 1991; Zheng et al., 2004). Some widely used indices are the Normalized Difference Vegetation Index (NDVI), Difference Vegetation Index (DVI), Ratio Vegetation Index (RVI), Greenness Index (GI), Soil Adjusted Vegetation Index (SAVI), Transformed SAVI (TSAVI), Modified SAVI (MSAVI), and Perpendicular Vegetation Index (PVI). The basis of most vegetation indices is the estimation of photosynthetically active radiation (Joel et al., 1997).

There are several distinct growth periods during a growing season and classification of vegetation characteristics depends on the presence or absence of vegetative cover and the condition of that vegetation at the time of the acquired image. Many researchers have mentioned that a significant correlation exists between spectral data and different vegetation growth parameters (Tucker, 1979; Thenkabail et al., 2004; Tian et al., 2007; Houborg and Boegh, 2008). Guerschman et al. (2003) recommended that, when possible, three images (spring, early-summer, late-summer) be used in the identification of summer crops, winter crops and rangelands. Using five Landsat TM image dates from a single year, Oetter et al. (2000) were able to create a map of 20 LULC classes. Lucas et al. (2007), comparing single and multi-date Landsat Enhanced Thematic Mapper (ETM+) images for vegetation classification, found that multi-date imagery allowed for a more accurate classification of different vegetation types. In another study, Maxwell et al. (2004) were able to identify four major LU types (bare soil/sparse vegetation, rangeland, urban, and riparian) and three crop types (corn, sorghum, and soybeans) using only bands 2 and 4 of a single late summer Landsat Multi-spectral Scanner (MSS) image.

The Iranian Forest, Range and Watershed Management Organization has been involved in mapping the LULC for the last 45 years using aerial photographs and topographic maps. Recently, satellite images have been used for such LULC classification, in a manner different from that proposed in this paper. The problems surrounding existing LULC maps are as follows: (i) Agricultural lands (irrigated farming and dry farming) have been mapped with visual interpretation techniques on optical image composites and field investigations. These polygon boundaries have been found to not be accurate and have overlapped with other classes. (ii) Further, on the same maps, an initial field investigation showed that low density forest and different rangeland classes have significantly overlapped. (iii) About 15% of the land area was classed as 'mixed'; separation into individual classes was not possible.

Because of the frequent difficulty in obtaining multi-date images for a single year for all the study areas of interest, the goal of the present study was to develop a new protocol for LULC classification using a large study area (4511.8 km^2) based on readily available ancillary information plus analysis of three single date Landsat ETM+ images. The study area chosen was the Golestan dam watershed in Iran.

2. Materials and methods

2.1. Study area

With an area of 4511.8 km^2, Iran's Golestan dam watershed is located between 55°21′ and 56°28′E longitude, and 36 44′ and 37°49′N latitude, in the northeast portion of Golestan Province (Fig. 1a). This sub-watershed of the Gorgan River watershed is composed of a complex combination of mountains, hills, plains and rivers. The highest elevation is 2492 m above mean sea level and the lowest elevation is 47 m. Because of its geographic situation and topography, a wide range of climates prevail across the different portions of the Golestan dam watershed: from semi-arid in the north-west and south to humid in the central portion (Fig. 1b). Mean annual precipitation ranges from 195 to 700 mm and mean annual air temperature from 8.5 to 17 °C. March is the month of greatest rainfall, and June to October are the dry months (Japan International Cooperation Agency, 2005; Lar Consulting Engineering, 2007).

Existing landform maps show roughly half (49.3%) of the Golestan dam watershed to be mountainous, with the remaining landforms being: 30,743.6 ha (6.8% of total area) river alluvial plains; 8,038.7 ha (1.8%) piedmont plains; 8654 ha (1.9%) gravelly fans; 33,664.2 ha (7.5%) upper terraces; 8230 ha (1.8%) river terraces; and 139,630 ha (30.9%) hills (Saadat et al., 2008). Different sedimentary rocks such as limestone, sandstone, shale, dolomite, marl along with conglomerate, loess sediments and alluvium underlay the area (Banaei, 1993). Located in this area, the 920 km^2 Golestan Forest National Park has been recognized by UNESCO as part of the international network of Biosphere Reserves (Japan International Cooperation Agency, 2005). Agriculture is also an important sector in the Golestan dam watershed. The main crops are wheat (*Triticum æstivum* L.), barley (*Hordeum vulgare* L.), sunflower (*Helianthus annuus* L.), watermelon (*Citrullus lanatus* (Thunb.)), rice (*Oryza sativa* L.) and cotton (*Gossypium hirsutum* L.) (Banaei, 1993). Accelerated soil erosion, high sediment yields, floods and debris flow are serious problems in the Golestan dam watershed (Sharifi et al., 2002; Japan International Cooperation Agency, 2005).

2.2. Materials

The following image and map materials were used in this study:

(i) Growing season Landsat ETM+ images: spring (10 May, 2003), summer (20 July, 2000), and late-summer (09 September, 2001). It should be noted that the images are from different years, but lack of availability necessitated this limitation. As such, for this study it was assumed that the images are representative of their respective seasons.
(ii) 1:25,000 scale digital topographic maps with 10 m contour lines prepared by the National Cartographic Center of Iran and the Forest, Range and Watershed Management Organization (based on 1993 aerial photos). These were mainly used for geo-referencing satellite images and for some ground-truthing.
(iii) Two digital ancillary layers were also collected to assist in the interpretation and classification of the remotely sensed data. These were a 1:25,000 scale landform map prepared by Saadat et al. (2008), and a 1:50,000 scale climatic zone map based upon de Martonne's dryness index, prepared by Lar Consulting Engineering (2007).
(iv) Ground-truthing was collected for the purpose of supervised and NDVI classification and classification accuracy assessment. These data were collected in the same month as each image was acquired (May, July and September), but 4–6 years after the images were taken (details below).
(v) ERDAS Imagine (version 8.7) and ArcInfo (version 9) software were used for image classification and data analyses.

2.3. LULC classification and mapping

2.3.1. General description

LULC classification is one of the most widely used applications in remote sensing. The most commonly used approaches include unsupervised classification, supervised classification, image segmentation and NDVI. Each of these methods has their own

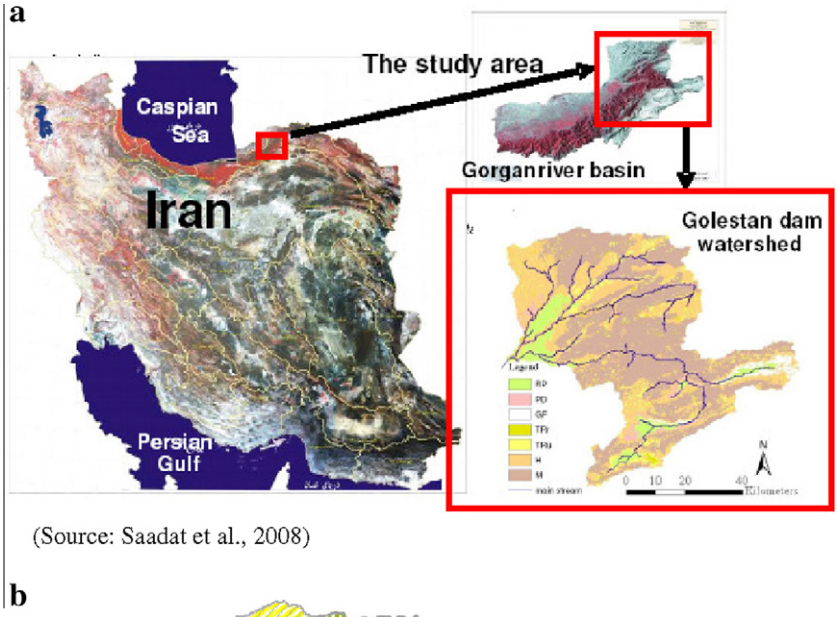

Fig. 1. The study area (a) location, (b) climatic zones.

restrictions and advantages. However, none of them individually can create an acceptable level of accuracy in producing LULC maps. Using the technique of object-based image segmentation, detailed information in the study area can be gathered effectively from the analysis of satellite images and certain ancillary data. In response to this, a new protocol was proposed in this research study as a way to combine the advantages of these methods and enhance the quality of LULC maps. The research methodology and proposed protocol have been shaped using a multidisciplinary and hierarchical approach.

For classification of each of the three Landsat ETM+ images, the study proceeded in five steps (Fig. 2): (i) preprocessing of the images, (ii) random extraction of a training sampling location: an unsupervised classification and two digital ancillary layers served in identifying potential LULC areas to aid in identifying sampling points, (iii) supervised classification of the image into LULC classes, (iv) enhancement of the LU classification via image segmentation and zonal statistics, and (v) enhancement of the LC classification via NDVI and climatic zones and creation of a final LULC map. Upon completion of all these processes the accuracy of the classifications were evaluated for each imaging date and comparisons were made.

2.3.2. Step i: Preprocessing of the images

An improved spatial resolution and geo-referenced Landsat ETM+ image for the study area was created. Landsat ETM+ images have 8 individual bands, each representing a single layer of continuous imagery. Given their low spatial resolution (60 m), the thermal bands (bands 6.1 and 6.2) were not used. The images' non-thermal bands (30 m) were combined into a multilayer image and clipped with a 150 m exterior buffer around the study area boundary (Fig. 2a, operations 1 and 2). Image fusion (or pan-sharpening) techniques have proven to be effective tools for providing better image information (Pohl and Van Genderen, 1998; Zhang, 2004). As such, because of the fragmented nature of the landscape, the 30 m data might not capture all details, and thus the 30 m multilayer image was fused with the 15 m panchromatic band (band 8) using the PCA method (Fig. 2a, operation 3). The PCA method was used because a major goal of this technique is to reduce data file

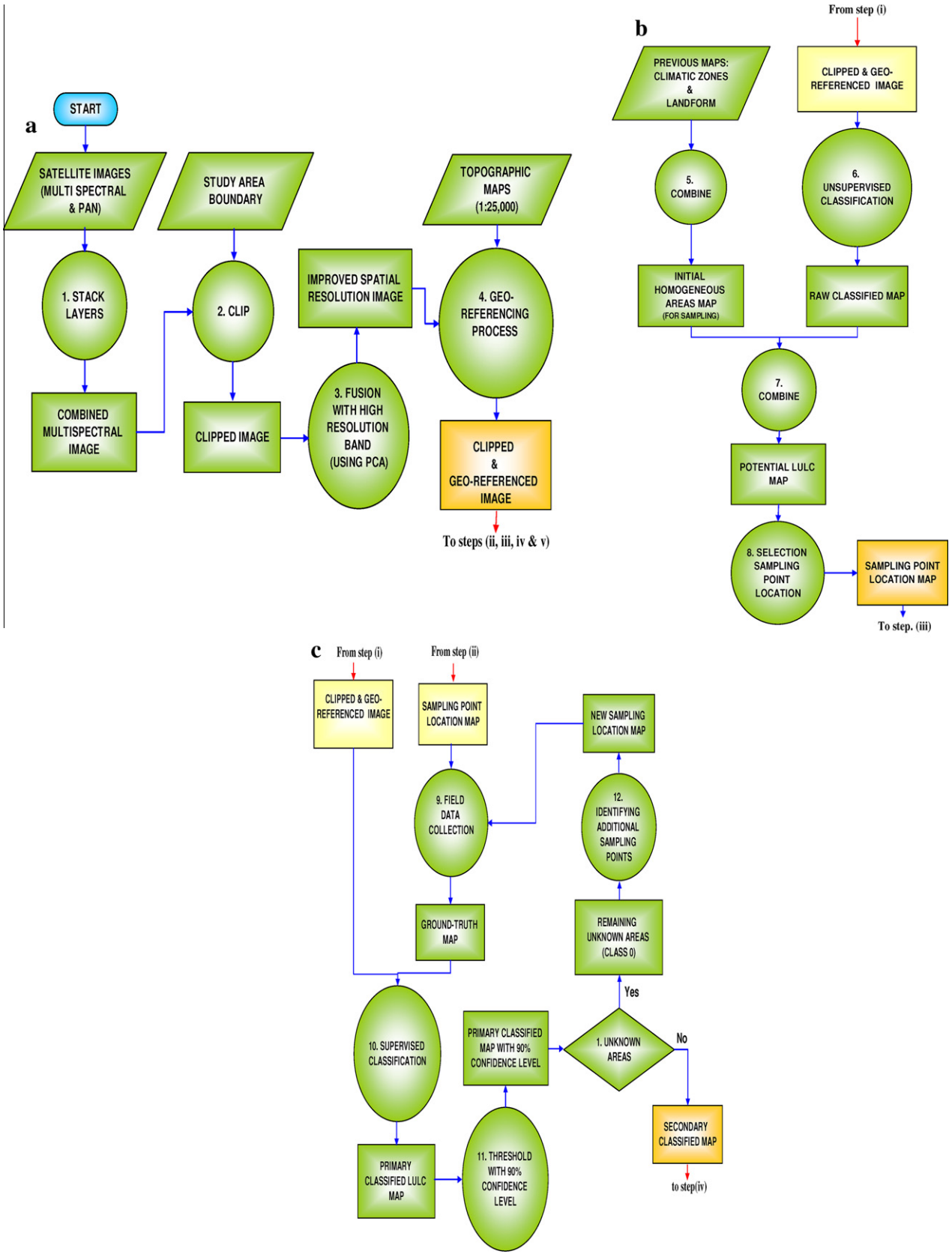

Fig. 2. Five steps of methodology: (a) preprocessing of the images, (b) extraction of a sampling point location map, (c) supervised classification of the image into LULC classes, (d) image segmentation and zonal statistics, (e) enhancement of the LC classification and creating a final LULC map. Circles = operation, Trapezoids = data input, Rectangles = maps or coverages and Diamonds = decisions.

size yet retain the spectral information of the six ETM+ bands (1–5, 7). This algorithm is mathematically rigorous (Welch and Ehlers, 1987). Geo-referencing was carried out for the image using 160 ground control points taken from 1:25,000 topographic maps

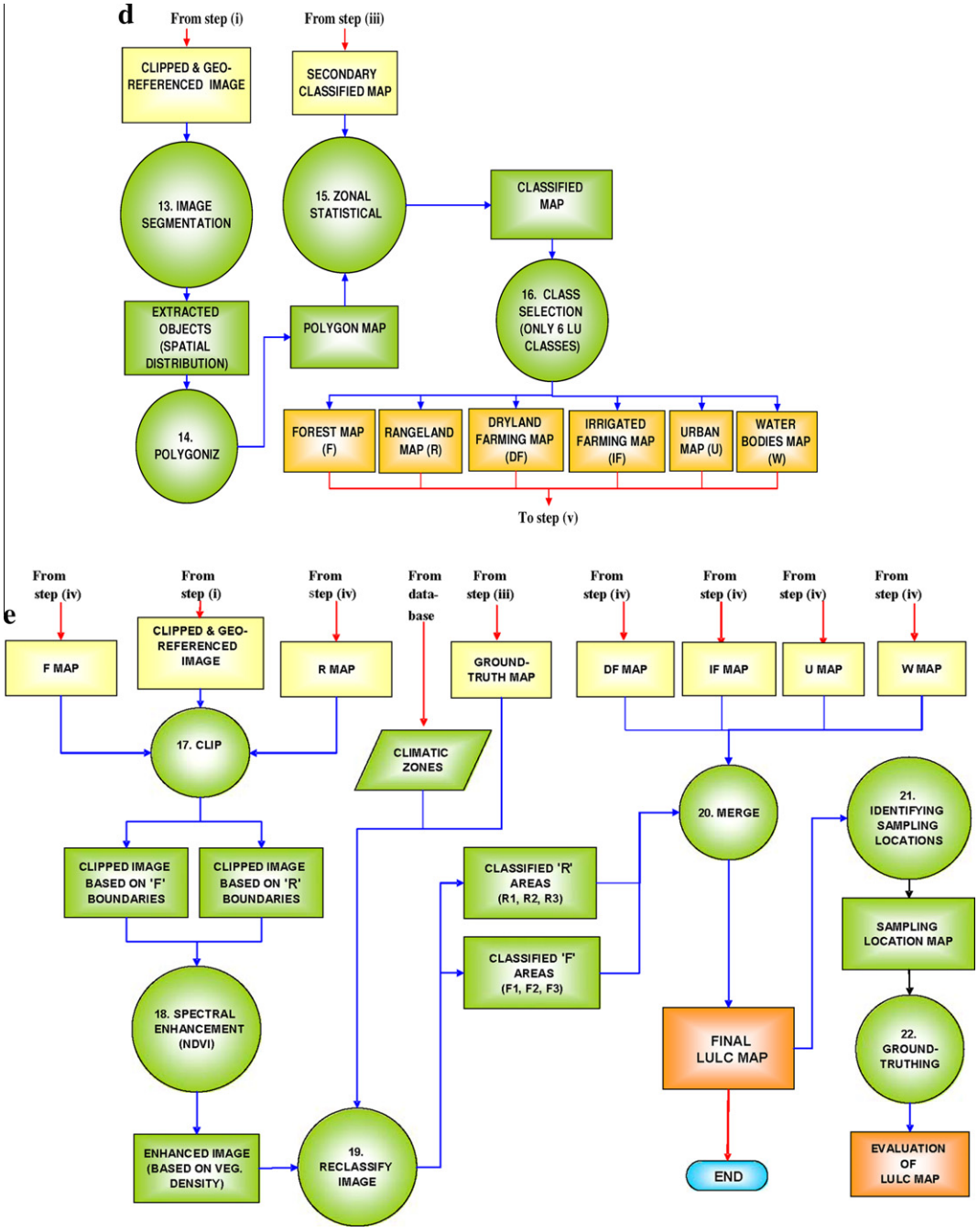

Fig. 2 (*continued*)

(Fig. 2a, operation 4). The coordinate system used in the topographic maps was the Universal Transverse Mercator (UTM) zone 40 with spheroid and datum WGS84.

2.3.3. Step ii: Extraction of a training sampling location map

Training sampling locations were chosen to encompass a full variety of potential LULC classes across the entire study area. Since this study encompassed a relatively large watershed (>4500 km^2), with different climatic zones and a complex combination of mountains, hills, and plains, two ancillary layers (4 climatic zones and 7 landform types, see Section 2.2) were combined to generate a map of 24 unique 'initial homogeneous areas' (Fig. 2b, operation 5). Concurrently, on each Landsat ETM+ image the Iterative Self-Organizing Data Analysis Technique (ISODATA) was performed. This is a type of unsupervised classification, and based on the natural groupings of pixels. Based on this method, applying a 95% convergence threshold and maximum iterations of 12 resulted in the generation of a raw classification map with 25 classes (Fig. 2b, operation 6). This map was then overlaid with the 'initial homogeneous areas' map (Fig. 2b, operation 7) creating a potential LULC (homogenous areas) map with 195 classes. Since each driven class has similar characteristics (similar land form, climate zone and spectral range), this map was used in an important supportive role for identifying appropriate training sampling locations across the entire study area. Based on these homogeneous areas, the 485 training sampling locations were extracted (Fig. 2b, operation 8) using a stratified random sampling procedure as described by Stehman (1999). Thirteen of these sites were essentially inaccessi-

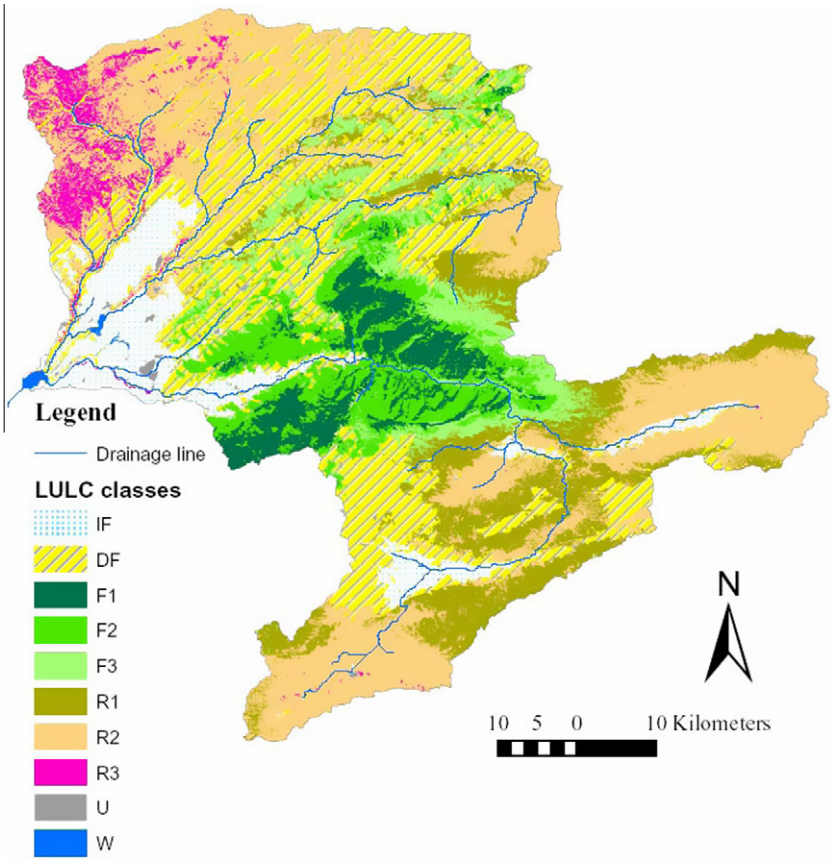

Fig. 3. LULC map derived from late-summer Landsat ETM+ image.

ble due to physical barriers or remoteness from roads. These were then replaced by 13 more accessible sites with the same classes. Because urban areas and water bodies represent less than 1% of the total area and they are easily recognized visually on the images, these entities were ignored for field visits.

2.3.4. Step iii: Supervised classification of the image into LULC classes

Ten classes were used for the supervised classification to generate an LULC map. LU was classified into 6 categories as follows: irrigated farming (IF), dryland farming (DF), forest (F), rangeland (R), urban (U), and water bodies (W). Then, according to vegetation density, F and R were further classified into LC: high density forest (F1, cover >70%), medium density forest (F2, 40% < cover $\leqslant$ 70%), and low density forest (F3, cover $\leqslant$40%); high density rangeland (R1, cover >30%, mostly between 30% and 50%), medium density rangeland (R2, 15% < cover $\leqslant$ 30%), and low density rangeland (R3, cover $\leqslant$15%). Thus there are 10 LULC classes in all; six land uses with two of these (F and R) being sub-classified into three vegetation cover densities.

To obtain the required ground-truth data for supervised classification, extensive field information was collected at the same 485 locations stipulated above in the same month as that in which each Landsat ETM+ image was acquired (May, July and September). A topographic road map (1:25,000) and a GPS unit were used to visit each location and without prior knowledge the location was placed into one of the 10 LULC classes (Fig. 2c, operation 9). In order to obtain the best possible results, these sampling locations were visited by experienced agronomists with local knowledge. The data collected were averaged over an area immediately surrounding each location point representing 9–25 image pixels. With this ground-truth data a maximum likelihood supervised classification was performed using an area of up to 100 pixels. At this stage, a primary classified LULC map for each of the three images with 10 classes was created (Fig. 2c, operation 10). In order to increase the accuracy of these maps a χ^2 threshold at a 90% confidence level was applied to the results. This process identified 1,205,324 pixels (6% of the total pixels) which had a 10% or greater chance of being misclassified. These pixels were put into class '0' and defined as 'unknown' areas (Fig. 2c, operation 11 and decision #1). Within these unknown areas, 26 additional random field location points were selected to visit (Fig. 2c, operations 12). Again a supervised classification was applied to the original 485 locations plus these 26 additional locations (Fig. 2c). Then a 90% confidence level analysis was repeated and an area of 183,276 pixels was identified as "unknown". Since this area encompassed only small pixel groups and in all represented less than 1% of the total area, this data was left as classified. The resulting image was termed the 'secondary classified map' (Fig. 2c, output).

2.3.5. Step iv: Image segmentation and zonal statistics

In an effort to further increase classification accuracy, an image segmentation algorithm was applied to the Landsat ETM+ images (Fig. 2d, operation 13 and 14) using the Bonnie Ruefenacht algorithm (Ruefenacht et al., 2002). This method classifies raster images based on pixel values and locations. All 6 bands of ETM+ were used in this process. The region size was set at 5 pixels and the Spectral Threshold Distance was set at 8 via trial and error, the aim being to maintain data integrity while also optimizing computer processing time and feature extraction. The resulting segmented image was then combined with the 'secondary classified map' of Fig. 2c. Image segmentation is able to separate objects of varying size, shape and homogeneity. The main task of image

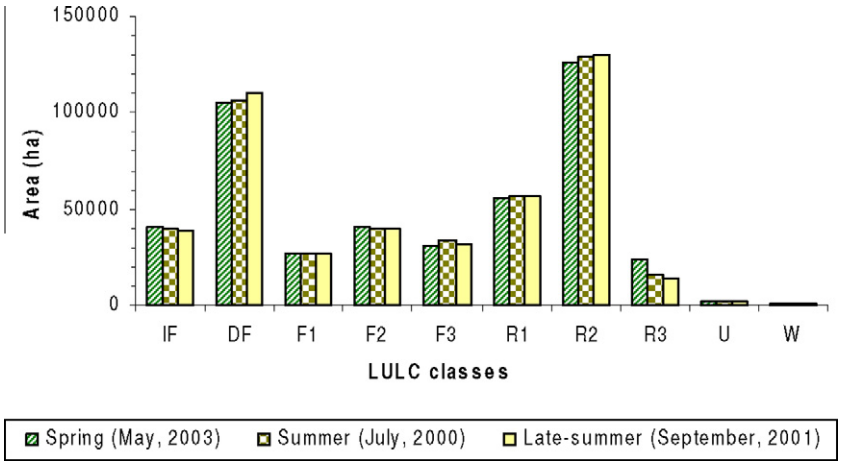

Fig. 4. The area of LULC classes using Landsat ETM+ images acquired in spring, summer, and late-summer.

Table 1
Error matrix of classification process of the Landsat ETM+ imagery of 10 May, 2003.

LULC	Ground-truth data								New classified	User's accuracy (%)
	IF	DF	F1	F2	F3	R1	R2	R3		
IF	**78**	8	1	1	1	0	2	1	**92**	85
DF	6	**146**	0	0	2	11	10	3	**178**	82
F1	2	0	**49**	0	0	0	0	0	**51**	96
F2	2	0	1	**73**	2	0	0	0	**78**	94
F3	0	5	0	3	**81**	0	0	0	**89**	91
F (Total)	4	5		209			0		218	96
R1	1	7	0	0	6	**72**	9	2	**97**	74
R2	0	12	0	0	0	10	**126**	5	**153**	82
R3	0	8	0	0	0	5	18	**42**	**73**	58
R (Total)	1	27		6			289		323	89
Total sites visited	**89**	**186**	**51**	**77**	**92**	**98**	**165**	**53**	**811**	
				220			316			
Producer's accuracy %	88	78	96	95	88	73	76	79		
				95			91			

Overall accuracy (OA) for LULC classification = 82%.
Overall accuracy (OA) for LU classification = 89%.

Table 2
Error matrix of classification process of the Landsat ETM+ imagery of 20 July, 2000.

LULC	Ground-truth data								New classified	User's accuracy (%)
	IF	DF	F1	F2	F3	R1	R2	R3		
IF	**80**	8	1	0	1	0	0	0	**90**	89
DF	5	**156**	0	0	0	1	4	2	**168**	93
F1	2	0	**50**	1	1	0	0	0	**54**	93
F2	2	0	0	**75**	1	0	0	0	**78**	96
F3	0	5	0	1	**85**	3	1	0	**95**	89
F (Total)	4	5		214			4		227	94
R1	0	0	0	0	4	**92**	2	0	**98**	94
R2	0	7	0	0	0	2	**152**	2	**163**	93
R3	0	10	0	0	0	0	6	**49**	**65**	75
R (Total)	0	17		4			305		326	94
Total sites visited	**89**	**186**	**51**	**77**	**92**	**98**	**165**	**53**	**811**	
				220			316			
Producer's accuracy %	90	84	98	97	92	94	92	92		
				97			96			

Overall accuracy (OA) for LULC classification = 92%.
Overall accuracy (OA) for LU classification = 93%.

segmentation was to create a set of non-overlapping segments (polygons). This algorithm merges groups of pixels into polygon objects (raster to vector format) but it is unable to classify them, thus the need for combining the images (the segmented ETM+

Table 3
Error matrix of classification process of the Landsat ETM+ imagery of 09 September, 2001.

LULC	Ground-truth data								New classified	User's accuracy (%)
	IF	DF	F1	F2	F3	R1	R2	R3		
IF	**88**	0	0	1	1	0	1	0	**91**	97
DF	1	**180**	0	0	0	3	3	1	**188**	96
F1	0	0	**51**	0	0	0	0	0	**51**	100
F2	0	0	0	**75**	0	0	0	0	**75**	100
F3	0	0	0	1	**88**	3	0	0	**92**	96
F (Total)	0	0		215			3		218	99
R1	0	0	0	0	3	**91**	9	2	**105**	87
R2	0	2	0	0	0	1	**150**	5	**158**	95
R3	0	4	0	0	0	0	2	**45**	**51**	88
R (Total)	0	6		3			305		314	97
Total sites visited	**89**	**186**	**51**	**77**	**92**	**98**	**165**	**53**	**811**	
				220			316			
Producer's accuracy %	99	97	100	97	96	93	90	85		
				98			96			

Overall accuracy (OA) for LULC classification = 95%.
Overall accuracy (OA) for LU classification = 97%.

and the secondary classified map) with zonal statistical analysis (Fig. 2d, operation 15). The zonal statistics present a distribution of each LULC within each segmented polygon. The reason for image segmentation is to use the resultant polygon vector map in combination with the supervised classification raster map and zonal statistics to generate a new classified polygon map. The idea behind this is to eliminate mixed pixels. It was found that for the six LU classes, the majority distribution was always more than 90% within any one segmented polygon. Thus each segmented polygon was fully classified to the 90% majority creating one layer for each of the six LU classes (Fig. 2d, operation 16).

2.3.6. Step v: Enhancement of the LC classification and creation of a final LULC map

For the LC classes (F1, F2, F3, R1, R2 and R3) another approach was required since in this case the results of the majority distribution classification via zonal statistics were much lower than 90%. To address this, each Landsat ETM+ image was clipped so as to show only the R and F entities as defined by the results of step iv. Subsequently, an NDVI was applied to both (Fig. 2e, operations 17 and 18). From the original 511 (485 + 26) ground-truth locations, 128 were known to be F and 241 were known to be R. Using these ground-truth values, NDVI values for each satellite image were grouped into six ranges; F1, F2, F3 and R1, R2 and R3. The results of the NDVI values (shown below in Section 3.1) for F showed little overlap. However R1, R2, and R3 had significant overlap. Thus an additional factor, 'climate', was introduced (Fig. 2e, operation 19). It was found that by grouping the R1, R2 and R3 values into temperate-semi-arid, cool-semi-arid, sub-humid and humid zones (Fig. 1b), much of the data overlap was eliminated. The resulting layers (F1, F2, F3, R1, R2 and R3) were merged with the IF, DF, U and W class maps (Fig. 2e, operation 20) to generate a final LULC map (Fig. 3).

2.3.7. Map accuracy assessment

To evaluate the accuracy of the LULC map, reference sampling locations were chosen to encompass a full variety of LULC classes across the whole study area. Since this study encompassed a relatively large watershed of 451,183 ha which included a variety of climatic conditions, the LULC map was overlaid with the climatic zones such that a full range of conditions would be sampled. This overlay map was used for identifying appropriate reference sampling locations across the entire study area. In total, 811 sites were extracted based on the stratified random sampling procedure as described by Stehman (1999). Class decisions were based on observing an area around the sampling location equal to 9–25 image pixels. These sampling locations were visited by experienced agronomists with local knowledge. Statistically, all 811 sites should have been visited, but the watershed is so large and some areas so remote that 18 sites had to be replaced with more accessible locations.

Finally, an error matrix was generated comparing land cover classifications from the map and the ground-truth classifications. The extent to which these two classifications agree was defined as the map accuracy according to the procedure of Congalton (1991). It should be noted that the field reference data was collected in the same month as each image yet acquired from 4 to 6 years after the image was taken. To address the issue of LULC changes that may have occurred over this time, local farmers were interviewed. The interviewed farmers were able to categorically state information about land use changes from the time of image acquisition up to now, so this information was used (LU changes were few; about 0.3%). As for vegetation conditions in the past, they were less certain and thus this information was not used.

3. Results and discussion

3.1. Results

Upon completion of all steps in Section 2.3 a final LULC map was created (the late-summer image, which yielded the classification result shown in Fig. 3). The area of LULC classes for the study area using Landsat ETM+ images acquired in spring, summer, and late-summer are shown in Fig. 4. Low density rangeland (R3) presented the widest variance (32–42%) in area values between spring, summer, and late-summer Landsat ETM+ images. Variance in area values for F3, IR, DF and R2 were 6–10%, 2–5%, 1–5% and 2–3%, respectively. The least variance between seasons was obtained for F1, F2 and R1 (all less than 1.5%).

Based on ground-truthing, the accuracy of the three finalized LULC maps derived from the Landsat ETM+ images acquired in spring (10 May, 2003), summer (20 July, 2000), and late-summer (9 September, 2001) was evaluated. For each of these images, an error matrix was generated (Tables 1–3). The accuracy parameters were calculated according to the procedure of Congalton (1991). Note that since U and W represent less than 1% of the total area (Fig. 4), they were excluded from any accuracy analysis. The producer's accuracy (PA) is a measure of how correct a classification is. As presented in Fig. 5a, LULC PA ranged from a low of 73% in

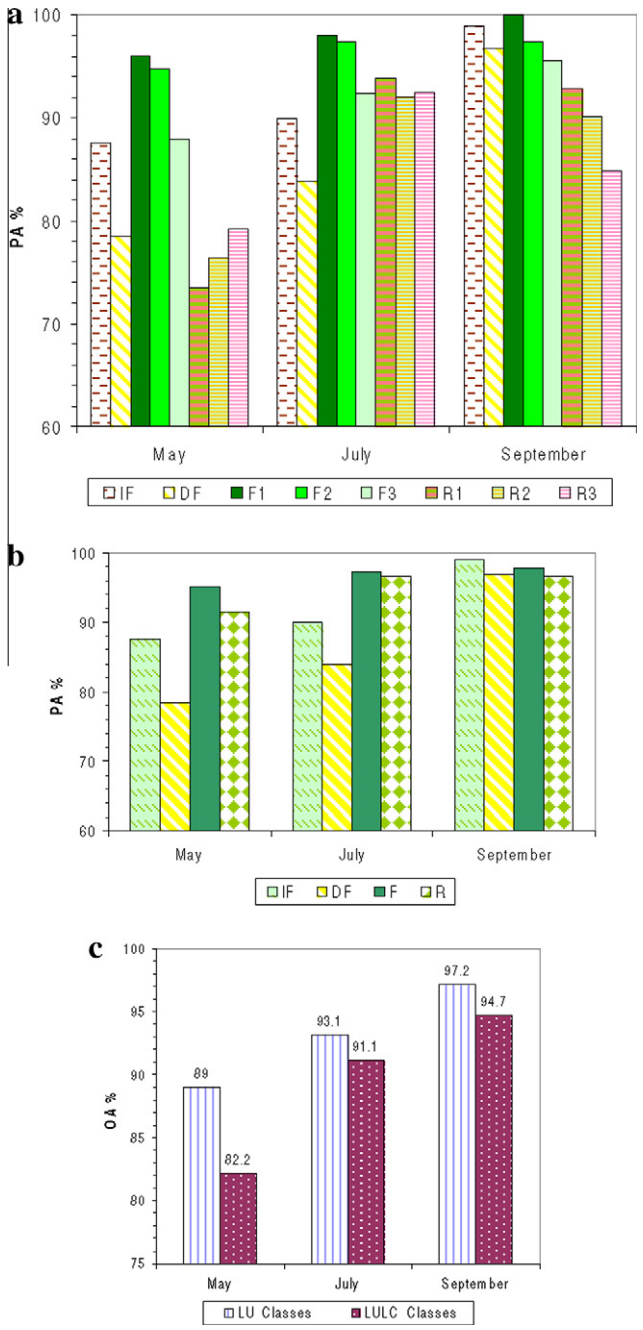

Fig. 5. The accuracy of the finalized LULC and LU maps derived from the Landsat ETM+ images acquired in spring (May, 2003), summer (July, 2000), and late-summer (September, 2001), (a) PAs of the LULC classification, (b) PAs of the LU classification, (c) OAs of the LULC and LU maps.

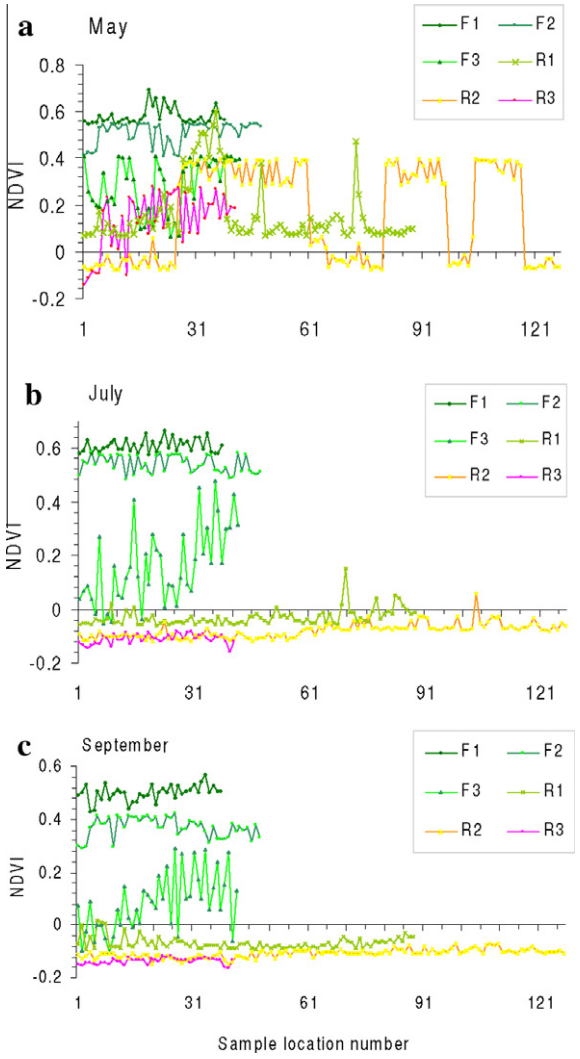

Fig. 6. The NDVI values for all sample locations in F and R based upon the Landsat ETM+ images acquired in (a) spring (May, 2003), (b) summer (July, 2000), and (c) late-summer (September, 2001).

the case of R1 (using the Landsat ETM+ imagery acquired in spring) to a high of 100% in the case of F1 (using Landsat ETM+ imagery acquired in late-summer). Values for the remaining four LU classes (before F and R were divided into LC classes) ranged from a low of 78% in the case of DF (using Landsat ETM+ imagery acquired in spring) to a high of 99% (Fig. 5b) in the case of IF (using Landsat ETM+ imagery acquired in late-summer). The user's accuracy (UA) is a measure of how well the classification process captured all occurrences of any of the eight LULC types (excluding U and W); this ranged from a low of 58% (Table 1) in the case of R3 (using Landsat ETM+ imagery acquired in spring) to a high of 100% (Table 3) in the case of F1 and F2 (using Landsat ETM+ imagery acquired in late-summer). UA for the four LU classes ranged from a low of 82% (Table 1) in the case of DF (using Landsat ETM+ imagery acquired in spring) to a high of 99% (Table 3) in the case of F (using Landsat ETM+ imagery acquired in late-summer). For comparison, Lucas et al. (2007) classified forest, marshy grasslands, bracken, dry heath, and semi-improved grasslands with a PA of 100%, 65%, 62%, 48% and 47%, respectively, using multi-date Landsat ETM+ imagery.

In general, the highest PAs and those which varied the least between seasons were obtained for F, indicating that forests are the easiest to identify (Fig. 5a and b). In the same figure, PA values for DF, IF, and R tended to show greater variance between spring, summer, and late-summer Landsat ETM+ images. Sivanpillai et al. (2007) were also able to classify forested areas better than non-forested areas using AVHRR imagery.

3.2. Single date imagery discussion

Referring to Fig. 5c, the late-summer (09 September, 2001) Landsat ETM+ imagery presented the best overall results, with an overall accuracy (OA) of 95% for LULC classes and 97% for LU classes. The spring (10 May, 2003) Landsat ETM+ imagery presented the poorest results with an OA of 82% for LULC classes and 89%

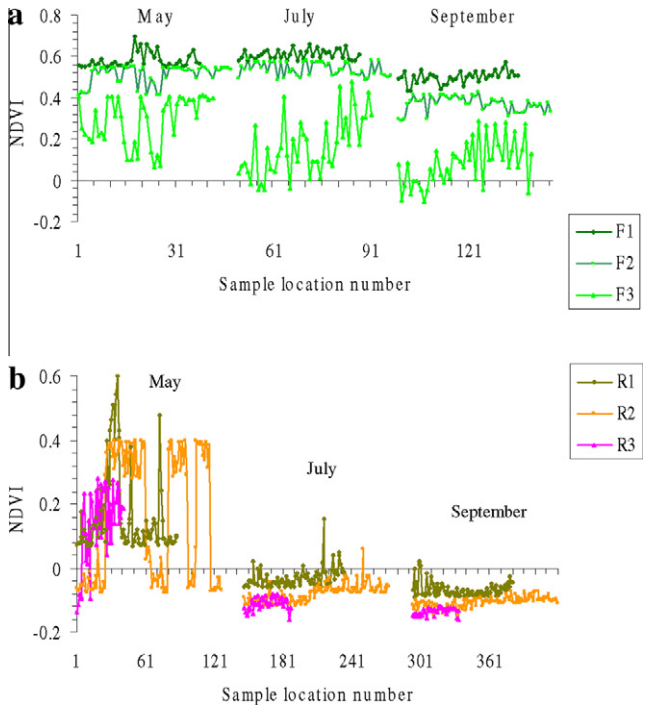

Fig. 7. The NDVI values based upon the three image times (spring, summer and late-summer) for (a) sample locations in F1, F2 and F3, (b) sample locations in R1, R2 and R3.

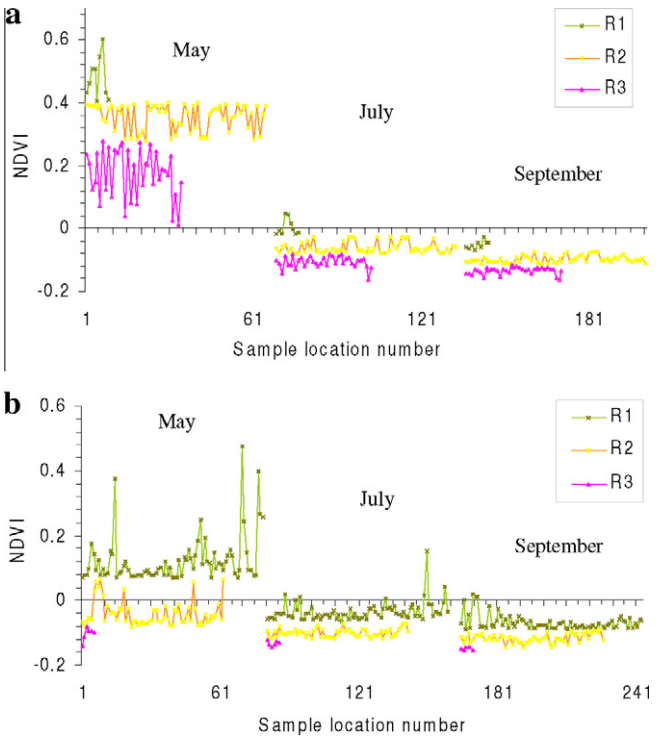

Fig. 8. Grouping NDVI values (based upon the three image times) of R1, R2 and R3 sample locations into two climatic zones (a) temperate-semi-arid zone (b) cool-semi-arid, sub-humid, and humid zones.

for LU classes. The summer (20 July, 2000) Landsat ETM+ imagery presented intermediary results with an OA of 91% for LULC classes and 93% for LU classes. Similarly, Sedano et al. (2005), using MODIS imagery in southern Africa, found that late summer gave the best results and spring the poorest.

The spring Landsat ETM+ imagery produced the least accurate results, particularly with respect to R (R1, R2 and R3) and DF. This is likely the result of two factors. At low elevations, spring is well advanced and what will become R3 is, in the spring, due to March rains, and infested with weeds thus making it seem like R1. Furthermore, at high elevations spring has not yet arrived and the grazing of the previous year tends to make R1 look like R3. And finally, R, DF, and IF are all, in the early spring, infested with weeds to a similar degree. Plowing, irrigation and grazing, all of which impact weed populations differently, have not as yet occurred. For example, in the column under DF (Table 1), of the 186 sites visited, 27 are mis-classed as R and eight as IF.

Using the summer (20 July, 2000) Landsat ETM+ imagery allowed for better discrimination of R (R1, R2 and R3) than did the spring image. However, the values for DF and IF (84% and 90%, respectively) were still consistently below the OA (91%). This is likely because wheat and barley (both occurring on both DF and IF) are harvested in June and July thus making them both look like DF once harvested. Cotton (IF), watermelon (DF), and sunflowers (mostly DF) are sown from April to mid June (spring) and harvested in late July to mid October. The long period of planting for these crops results in a relatively large variation of reflectance for each during the summer period, making differentiation difficult.

Using the late summer (09 September, 2001) Landsat ETM+ imagery allowed for the best discrimination of DF and IF with a PA of 97% and 99%, respectively. This was due to the fact that at this time of year most crops at different locations in the study area are harvested. The reflectance values obtained are thus for soil, and not vegetation reflectance, and IF soils would likely have a distinctly higher moisture content than DF soils, making them relatively easy to differentiate. The values of PA for R1, R2 and R3 (93%, 90% and 85%, respectively) using the late-summer Landsat ETM+ imagery were below the OA (95%). This is likely the result of overgrazing which is common in the area. By the end of the season overgrazing will make R1 look like R3. Further, due to overgrazing, R3 can look like DF. It can be seen that local agronomic knowledge is helpful in understanding relative classification accuracies.

3.3. NDVI value analysis

Because LC classes (F1, F2, F3, R1, R2 and R3) were the most difficult to discriminate, plots of NDVI values for all ground-truth locations for F and R were created (Fig. 6). The first thing that is evident from these plots is that F1, F2 and F3 exhibit little to no overlap. Thus NDVI is sufficient for differentiating F1, F2 and F3, if F is first isolated from R (Fig. 7a). R1, R2 and R3 do show significant overlap (Fig. 7b), thus a parameter in addition to NDVI is required for differentiation. By trial and error it was found, for all images, that by grouping R1, R2 and R3 plots into two climate zones (one temperate-semi-arid and the other all other climatic zones clumped together), differentiation was improved. This improvement likely occurs because vegetation is dependent on climate and rangeland vegetation is rapidly dynamic due to climate compared to forest vegetation.

Fig. 7a shows that F3 (low density forest) has the widest variance in NDVI values compared to F1 and F2. This is as expected since F1 and F2 present a more uniform and dense canopy cover; F3 being sparsely vegetated comes closest to and is most easily confused with R1. Also, the average NDVI value for all F1, F2 and F3 decreases over the season (with F3 the most). It is likely that F3 decreases the most because some of the reflectance in F3 is due to shrubs, which would on average dry out over a dry growing

season more than trees would. Further, some F3 is used for grazing while F1 and F2 are not.

Fig. 8a and b show that NDVI values for R1, R2, and R3 have the widest variance in spring, and that NDVI values decrease over the season with the vast majority of this decrease occurring in early summer. These results are to be expected since spring is the time of highest vegetation (for rangeland), yet with the lack of rain and overgrazing in summer the vegetation is quickly reduced. The lower NDVI values from summer and late summer show that R1, R2 and R3 have, for a long time, relatively low vegetation cover (relative to IF and F).

Other studies have also used a number of ancillary layers such as climatology and topography to aid in the identification of vegetation types (Belda and Melia, 2000; Homer et al., 2007; Lucas et al., 2007). In our study, a landform map and climatic zones were used to assist in the interpretation and classification of remotely sensed data for LULC. The results show that successful mapping depends on more than just the analysis of reflectance information. Incorporating climatic and topographic conditions helped delineate what was otherwise overlapping information. Subsequently, knowledge of local vegetation conditions such as the occurrence of weeds in spring and shrubs within F3 helped to interpret variance and the level of reflectance observed.

4. Conclusions and recommendations

This study encompassed a relatively large watershed of 451,183 ha which included a variety of vegetation cover from high density forest to low density rangeland. Accurate LULC maps can play an important role in aiding watershed management as well as helping in deciding what sort of lands are best suited for sustaining agriculture and in what manner this agriculture should be practiced. In this study, in order to extract and identify various LULC classes, Landsat ETM+ images from the growing season (spring, summer and late summer) were used. Further, a landform map and climatic zones were used to assist in the interpretation and classification of the remotely sensed data.

This study proposed the use of a unique combination of proven classification steps to create a successful protocol for accurately classifying LULC types. The protocol enhances initial reflectance based classification with the use of image segmentation and supplemental segregation via the use of ancillary information (climatic and landform). The results show that accurate classification depends on more than just analysis of reflectance information. Specifically, incorporating climatic and landform information helps increase LU classification accuracy and NDVI can be used to separate overlapping LC classifications.

This study illustrated that the highest producer's accuracies (PA) and those which varied the least between seasons were obtained for F, indicating that forests are the easiest to identify. Low density forest (F3) had the widest variance in NDVI values compared to F1 and F2. This is as expected since F1 and F2 present a more uniform canopy cover. Further, some F3 is used for grazing while F1 and F2 are not. NDVI values from summer and late summer images were consistently lower for R1, R2 and R3 when compared to IF and F, and the largest portions of NDVI decrease occurred from spring to summer, with little further decrease into late summer.

The study corroborates other studies, finding that late summer images present the best information for LULC classification (OA of 95%). It was found that knowledge of local agronomic conditions helps interpret reflectance variance within a classification and change of reflectance within a classification over the growing season.

Since similar ancillary layers (climate and landform maps) and Landsat ETM+ images (and also ASTER images or other potential multi-spectral images with medium spatial resolution) are available for all of Iran, it is recommended that the new protocol presented in this paper be applied in different geographic locations in Iran. Because many of the processes used in this classification protocol, like the hierarchy of classes and multiple layers of segmentation and classification (some of which are driven by thematic and not only spectral data) are actually embedded in the new paradigm of digital image interpretation known worldwide as object-based image analysis (OBIA), it is recommended that other available and powerful computing tools and a genuine object-based image analysis guided by a semantic network be used in these areas and the results be validated. It is also recommended that in the future, additional research be conducted on the support vector machine (SVM) method, which has a robust algorithm, to increase accuracy during the classification process. The results of these studies will make it clear if this method can be considered universal for developing LULC maps. Further, it is expected that knowledge of local vegetation conditions (specific vegetation cover types, and when during the growing season they occur and at what elevation) and knowledge of human interventions such as grazing and irrigation can help interpret reflectance variance within a classification and the level of reflectance observed. It is therefore recommended that further studies such as this one incorporate the documentation of such factors. Use of such data could elicit new relationships between image reflectance and land management.

Acknowledgements

The authors gratefully acknowledge the Forest, Range and Watershed Management Organization of Iran and the Watershed Management Office of Golestan Province for providing data sets, facilities, manpower and field support for this study. Many thanks to Mr. Hossein Ali Mohammadi for his collaboration and for his significant contributions to the field work. We are grateful for the constructive comments given by Dr. Daniel L. Civco and three anonymous reviewers of our paper. Partial funding for this study came from the Natural Sciences and Engineering Research Council of Canada via an NSERC Discovery Grant held by Jan Adamowski.

References

Banaei, M.H., 1993. A report on soil survey, land classification and irrigation capability for a region located south of the Gorgan River. Publication No. 368, Soil and Water Research Institute of Iran, Tehran (in Farsi).

Belda, F., Melia, J., 2000. Relationships between climatic parameters and forest vegetation: application to burned area in Alicante (Spain). Forest Ecology and Management 135 (1–3), 195–204.

Cihlar, J., 2000. Land cover mapping of large areas from satellites: status and research priorities. International Journal of Remote Sensing 21 (6-7), 1093–1114.

Chust, G., Ducrot, D., Pretus, J.L., 2004. Land cover mapping with patch-derived landscape indices. Landscape and Urban Planning 69 (4), 437–449.

Cohen, Y., Shoshany, M., 2002. A national knowledge-based crop recognition in Mediterranean environment. International Journal of Applied Earth Observation and Geoinformation 4 (1), 75–87.

Congalton, R.G., 1991. A review of assessing the accuracy of classifications of remotely sensed data. Remote Sensing of Environment 37 (1), 35–46.

de Asis, A.M., Omasa, K., 2007. Estimation of vegetation parameter for modeling soil erosion using linear Spectral Mixture Analysis of Landsat ETM data. ISPRS Journal of Photogrammetry and Remote Sensing 62 (4), 309–324.

Focardi, S., Loiselle, S.A., Mazzuoli, S., Bracchini, L., Dattilo, A.M., Rossi, C., 2008. Satellite-based indices in the analysis of land cover for municipalities in the province of Siena, Italy. Journal of Environmental Management 86 (2), 383–389.

Guerschman, J.P., Paruelo, J.M., Di Bella, C., Giallorenzi, M.C., Pacin, F., 2003. Land cover classification in the Argentine Pampas using multi-temporal Landsat TM data. International Journal of Remote Sensing 24 (17), 3381–3402.

Hagner, O., Reese, H., 2007. A method for calibrated maximum likelihood classification of forest types. Remote Sensing of Environment 110 (4), 438–444.

Homer, C., Dewitz, J., Fry, J., Coan, M., Hossain, N., Larson, C., Herold, N., Mckerrow, A., VanDriel, J.N., Wickham, J., 2007. Completion of the 2001 National Land Cover Database for the Conterminous United States. Photogrammetric Engineering and Remote Sensing 73 (4), 337–341.

Homer, C., Huang, C., Yang, L., Wylie, B., Coan, M., 2004. Development of a 2001 National Land Cover Database for the United States. Photogrametric Engineering and Remote Sensing 70 (7), 829–840.

Houborg, R., Boegh, E., 2008. Mapping leaf chlorophyll and leaf area index using inverse and forward canopy reflectance modeling and SPOT reflectance data. Remote Sensing of Environment 112 (1), 186–202.
Jackson, R.D., Huete, A.R., 1991. Interpreting vegetation indices. Preventive Veterinary Medicine 11 (3–4), 185–200.
Japan International Cooperation Agency, 2005. The study on flood and debris flow in the Caspian coastal area focusing on the flood-hit region in Golestan province. Interim Report. Tehran, Iran, p. 302.
Joel, G., Gamma, J.A., Field, C.B., 1997. Production efficiency in sunflower: the role of water and nitrogen stress. Remote Sensing of Environment 62 (2), 176–188.
Joshi, P.K.K., Roy, P.S., Singh, S., Agrawal, S., Yadav, D., 2006. Vegetation cover mapping in India using multi-temporal IRS Wide Field Sensor (WiFS) data. Remote Sensing of Environment 103 (2), 190–202.
Labrecque, S., Fournier, R.A., Luther, J.E., Piercey, D., 2006. A comparison of four methods to map biomass from Landsat-TM and inventory data in western Newfoundland. Forest Ecology and Management 226 (1-3), 129–144.
Lar Consulting Engineering, 2007. The study on flood and debris flow in the Golestan province. Regional Water Board in Golestan, Ministry of Energy, Tehran, Iran, p. 425 (in Farsi).
Lucas, R., Rowlands, A., Brown, A., Keyworth, S., Bunting, P., 2007. Rule-based classification of multi-temporal satellite imagery for habitat and agricultural land cover mapping. ISPRS Journal of Photogrammetry and Remote Sensing 62 (3), 165–185.
Maxwell, S.K., Nuckols, J.R., Ward, M.H., Hoffer, R.M., 2004. An automated approach to mapping corn from Landsat imagery. Computers and Electronics in Agriculture 43 (1), 43–54.
Oetter, D.R., Cohen, W.B., Berterretche, M., Maiersperger, T.K., Kennedy, R.E., 2000. Land cover mapping in an agricultural setting using multiseasonal Thematic Mapper data. Remote Sensing of Environment 76 (2), 139–155.
Pohl, C., Van Genderen, J.L., 1998. Multi-sensor image fusion in remote sensing: concepts, methods and applications. International Journal of Remote Sensing 19 (5), 823–854.
Renard, K.G., Foster, G.R., Weesies, G.A., McCool, D.K., Yoder, D.C., 1997. Predicting soil erosion by water: a guide to conservation planning with the revised universal soil loss equation (RUSLE). Agriculture Handbook, vol. 703. US Department of Agriculture, Washington DC, p. 384.
Renschler, C., Harbor, J., 2002. Soil erosion assessment tools from point to regional scales the role of geomorphologists in land management research and implementation. Geomorphology 47 (2-4), 189–209.
Ruefenacht, B., Vanderzanden, D., Morrison, M., Golden, M., 2002. New technique for segmenting Images. An image segmentation algorithm developed by the USDA Forest service, Remote Sensing Application Center. Available from: <http://www.fs.fed.us/> (accessed 12.04.2011).
Saadat, H., Bonnell, R., Sharifi, F., Mehuys, G., Namdar, M., Ale-Ebrahim, S., 2008. Landform classification from a digital elevation model and satellite imagery. Geomorphology 100 (3–4), 453–464.
Sedano, F., Gong, P., Ferrao, M., 2005. Land cover assessment with MODIS imagery in southern African Miombo ecosystems. Remote Sensing of Environment 98 (4), 429–441.
Sharifi, F., Saghafian, B., Telvari, A., 2002. The great 2001 flood in Golestan province, Iran: Causes and consequences. In: Proceedings of the International Conference on Flood Estimation. March 6–8, 2002. Berne, Switzerland, CHR–KHR Report 11–17, pp. 263–271.
Sivanpillai, R., Srinivasan, R., Smith, C.T., Messina, M.G., Ben Wu, X., 2007. Estimating regional forest cover in East Texas using Advanced Very High Resolution Radiometer (AVHRR) data. International Journal of Applied Earth Observation and Geoinformation 9 (1), 41–49.
Stehman, S.V., 1999. Basic probability sampling designs for thematic map accuracy assessment. International Journal of Remote Sensing 20 (12), 2423–2441.
Thenkabail, P.S., Enclona, E.A., Ashton, M.S., Legg, C., De Dieu, M.J., 2004. Hyperion, IKONOS, ALI, and ETM+ sensors in the study of African rainforests. Remote Sensing of Environment 90 (1), 23–43.
Tian, Q., Luo, Z., Chen, J.M., Chen, M., Hui, F., 2007. Retrieving leaf area index for coniferous forest in Xingguo County, China with Landsat ETM+ images. Journal of Environmental Management 85 (3), 624–627.
Tucker, C.J., 1979. Red and photographic infrared linear combinations for monitoring vegetation. Remote Sensing of Environment 8 (2), 127–150.
Wardlow, B.D., Egbert, S.L., Kastens, J.H., 2007. Analysis of time-series MODIS 250 m vegetation index data for crop classification in the U.S. Central Great Plains. Remote Sensing of Environment 108 (3), 290–310.
Welch, R., Ehlers, W., 1987. Merging Multiresolution SPOT HRV and Landsat TM Data. Photogrammetric Engineering and Remote Sensing 53 (3), 301–303.
Zhang, Y., 2004. Understanding image fusion. Photogrammetric Engineering and Remote Sensing 70 (6), 657–661.
Zheng, D., Rademacher, J., Chen, J., Crow, T., Bresee, M., Le Moine, J., Ryu, S.R., 2004. Estimating aboveground biomass using Landsat 7 ETM+ data across a managed landscape in northern Wisconsin, USA. Remote Sensing of Environment 93 (3), 402–411.